Inorg. Chem. **2003**, *42*, 7830–7838

Structure and Physical Properties of 1D Magnetic Chalcogenide, Jamesonite ($FePb_4Sb_6S_{14}$)†

Yoshitaka Matsushita* and Yutaka Ueda

Materials Design and Characterization Laboratory (MDCL), Institute for Solid State Physics (ISSP), The University of Tokyo, 5-1-5 Kashiwanoha, Kashiwa, Chiba 277-8581 Japan

Received June 9, 2003

Monoclinic $FePb_4Sb_6S_{14}$ phase, jamesonite, which is a candidate material as a $S = 2$ Haldane compound, has been synthesized by the direct reaction of elements under dry conditions with sealed evacuated quartz tubes. The congruent melting point was determined at 592 °C by DTA measurements. Shiny metallic gray needle crystals grow on the surface of bulk heated at 550 °C. The elongated direction of each needle crystal is parallel to the *c*-axis. The crystal structure refinement ($P2_1/a$, $a = 15.750(6)$ Å, $b = 19.125(3)$ Å, $c = 4.030(4)$ Å, $\beta = 91.68(8)°$, $V = 1213(1)$ Å^3, $Z = 2$, $D_c = 5.651$ g/cm^3, $R_1 = 3.16\%$) reveals the presence of two rod substructures elongated parallel to the *c*-axis. One is the lozenge-shaped Bi_2Te_3-type (or called SnS archetype), $^3_\infty[Pb_4Sb_6S_{13}]$. The other is the novel single magnetic one-dimensional (1D) straight chain, $^1_\infty[FeS_6]$. This compound shows intrinsic semiconductor behavior in the electric conductivity measurements. The optical band gap, 0.48 eV, is estimated by near-IR diffuse reflectance measurements. In the magnetic susceptibility measurements, this compound shows 1D-Heisenberg antiferromagnetic behavior with a broad peak at ∼33.5 K, where Fe^{2+} takes the high-spin state, $t_{2g}^4e_g^2$. A possibility for the $S = 2$ Haldane system is discussed.

I. Introduction

Recently, the research of transition metal chalcogenides has been revived in solid-state chemistry because the dimensionality of the framework structures or doping level can control the ratio of cation to chalcogen atom in chalcogenides as has been achieved in oxides.[1] The chalcogenides have various kinds of specific physical properties and are in wide variety for applied materials in the next generation, such as thermoelectrics,[2] nonlinear optical materials,[3] photoelectrics,[4] phosphors,[5] and solid-state electrolytes for lithium secondary batteries.[6]

We have investigated the multinary chalcogenides which contain transition metals in anticipation of exciting new magneto-phenomena from the local dimensionalities and environments of transition metals. In magneto-chemistry and physics field, low-dimensional magnetic compounds are of great interest because of their peculiar properties caused by the quantum many body effects.[7] Particularly, one-dimensional Heisenberg antiferromagnetic (1D-HAF) chain compounds have been extensively researched because most of them are considered as a prototype in the statistic physics. In 1983, Haldane theoretically predicted that the 1D-HAF systems having integer spin quantum number ($S = 1, 2, ...$) should have a spin energy gap, called Haldane gap (Δ), between the ground state and the first excited state. On the other hand, in the case of half-integer spin quantum number ($S = {}^1/_2, {}^3/_2, ...$) systems, the energy levels are spin-gapless.[8] Since Haldane's prediction, extensive studies have been

* Author to whom correspondence should be addressed. Tel/Fax: +81-4-7136-3436. E-mail: chaos@issp.u-tokyo.ac.jp.

† Abstract published in *Abstracts for 50th Anniversary Meeting, Mineral. Soc. Japan*, Oct. 1−4, 2002, Osaka, Japan.

(1) (a)Kanatzidis, M. G.; Sutorik, A. *Prog. Inorg. Chem.* **1995**, *43*, 151. (b)Eichhorn, B. W. *Prog. Inorg. Chem.* **1994**, *42*, 139.

(2) (a)Rowe, D. M., Ed. *CRC Handbook of Thermoelectrics*; CRC Press: Boca Raton, FL, 1995. (b)Kanatzidis, M. G. *Semicond. Semimet.* **2001**, *69*, 51. (c) Chung, D.-Y.; Hogan, T.; Brazis, P.; Rocci-Lane, M.; Kannewurf, C.; Bastea, M.; Uher, C.; Kanatzidis, M. G. *Science* **2000**, *287*, 1024.

(3) Ballman, A. A.; Byer, R. L.; Eimerl, D.; Feigelson, R. S.; Feldman, B. J.; Goldberg, L. S.; Menyuk, N.; Tang, C. L. *Appl. Opt.* **1987**, *26*, 224.

(4) Ibuki, S.; Yoshimatsu, S. *J. Phys. Soc. Jpn.* **1955**, *10*, 549.

(5) Shionoya, S., Yen, W. M., Eds. *Phosphor Handbook*; CRC Press: Boca Raton, FL, 1999.

(6) (a)Matsushita, Y.; Kanatzidis, M. G. *Z. Naturforsch.* **1998**, *53b*, 23. (b)Kanno, R.; Hata, T.; Kawamoto, Y.; Irie, M. *Solid State Ionics* **2000**, *130*, 97.

(7) Miller, J. S. *Extended Linear Chain Compounds*; Plenum: New York/London, 1982; Vols. 1−3.

10.1021/ic034634t CCC: $25.00
Published on Web 10/25/2003

carried out on 1D-HAF systems with integer S. In the real system, the first compound showing $S = 1$ Haldane gap, $[Ni^{2+}(en)_2NO_2](ClO_4)$ (en = $C_2H_8N_2$) abbreviated as NENP, was discovered by Renard and co-workers in 1986. [9] NENP has a quasi-Ni^{2+}-linear 1D chain in the crystal structure, and its $\Delta_{S=1}/J$ estimated from measurements of anisotropic magnetizations is 0.41, where J (>0) is the nearest-neighbor exchange integral. After the discovery of this compound, many of the $S = 1$ Haldane gap compounds have been studied until now.[10] In the chalcogenide system, $Ag^+V^{3+}P_2S_6$ was reported to be an $S = 1$ (V^{3+}) Haldane gap compound.[11]

In the case of the $S \geq 2$ Haldane system, many researchers in chemistry and physics fields have been trying to find candidate compounds, but most of the candidates failed, partly because $\Delta_{S\geq 2}/J$ calculated by a numerical study are extremely too small to be experimentally observed compared with the $S = 1$ system. [For example, $\Delta_{S=2}/J = 0.08917(4)$ and $\Delta_{S=3}/J = 0.01002(3)$.][12] Finally, in 1996, the first $S = 2$ Haldane system compound, $Mn^{3+}Cl_3$(bipy) (bipy = $C_{10}H_8N_2$), was reported.[13] The $\Delta_{S=2}/J = 0.07(2)$ was estimated by anisotropic magnetic measurements.[13] Even at the present time, this is the only example of $S \geq 2$ Haldane systems.

In this study, we report the second $S = 2$ Haldane candidate quartenary sulfide, $Fe^{2+}Pb^{2+}{}_4Sb^{3+}{}_6S^{2-}{}_{14}$, which belongs to the jamesonite series in the *sulfosalt* group in mineralogy. The term *sulfosalt* means one sweepingly compositional category for multinary chalco-pnicogenate minerals, which are commonly used in the mineralogical field. In a broad sense, sulfosalts are regarded in mineralogy as compounds of metals and semi-metals with chalcogens. In chemistry, sulfosalts are known as derivatives from the hypothetical chalcoacids such as $H^+{}_3(Pn^{3+}Q^{2-}{}_3)$ etc. (Pn^{3+} = As, Sb, and Bi, and Q^{2-} = S, Se, and Te). The general formula commonly accepted for these minerals is $A_mPn_nQ_p$, where A are metal elements, Pn are semi-metal elements (formally trivalent), As, Sb, and Bi (partly Te^{4+}) only, and Q are chalcogens. Occasionally, a partial chalcogen site can be replaced by halogens and/or oxygen.

In nature, $Fe^{2+}Pb^{2+}{}_4Sb^{3+}{}_6S^{2-}{}_{14}$ has been found as the following two polymorphism minerals.[14]

1. jamesonite: monoclinic, $P2_1/a$

2. parajamesonite: orthorhombic?

Jamesonite has been commonly found as needle crystals in a hydrothermal vein associated with other sulfides such as pyrite (FeS_2), sphalerite (ZnS), galena (PbS), stibnite (Sb_2S_3), and others in nature, and also natural $FePb_4Sb_6S_{14}$ partially substitutes other minor elements such as Mn, Cu, Zn, and Se.[14] The studies for the jamesonite series minerals are, however, very limited. The reported studies are only rudimentary crystal structure analysis[15] and partial phase diagram study[16] for jamesonite. The primary crystal structure using limited intensity with natural jamesonite crystal was solved and refined to the isotropic temperature factor model by Niizeki and Burger in 1957.[15] In the structure, Fe^{2+} ($S = 2$) locates at the origin site (2a) and coordinates with six sulfur atoms. Each [FeS_6] octahedron forms the 1D-straight linear chain substructure that runs along the *c*-axis. The shortest Fe...Fe distances are 4 Å for intrachain and 12 Å for interchain, respectively. From this crystallographic point of view, jamesonite is expected to show the interesting 1D-HAF quantum spin behavior such as the $S = 2$ Haldane system.

In this study, we synthesize pure $Fe^{2+}Pb^{2+}{}_4Sb^{3+}{}_6S^{2-}{}_{14}$, which must resolve its crystal structure to characterize well the one-dimensionality of the iron magnetic chain and to understand well its physical properties from its crystal structure. Moreover, we try to clarify their physical properties such as thermal, optical, electrical, and magnetic properties systematically.

II. Experimental Section

Synthesis. We synthesized $FePb_4Sb_6S_{14}$ under dry conditions. A stoichiometric amount of elemental Fe (3N, Powder, Rare-Metallic Ltd.), Pb (5N+, Shot, Rare-Metallic Ltd.), Sb (5N+, Shot, Rare-Metallic Ltd.), and S (5N, Shot, Rare-Metallic Ltd.) was roughly mixed without any further treatments before use. The mixture was transferred to a quartz tube and was subsequently flame-sealed under vacuum ($\sim 10^{-5}$ Torr). The reaction was performed by the following two different heating methods.

Method A is a conventional heating method using furnaces. The tube was slowly heated to 500 °C over a 12-h period and then isothermed at this temperature for 3 days, followed by cooling to room temperature over 12 h. This primary product was re-ground up and again heated in the vacuum-sealed tube using a 550 °C furnace with a slight temperature gradient for an extra 3 days to make a pure compound. In this process, the temperature at the sample position in the furnace is 550 °C, and the end part is ~500 °C. The target compound of shiny metallic gray bulk together with needle-shaped crystals was obtained at the initial sample position.

Method B is the direct heating by flame. The slight Pb−Sb−S-rich starting material put in an evacuated quartz tube was moderately heated by a direct flame and melted completely. The melt was stirred by shaking gently for a good mixing and then quenched to room temperature. This is a good method to synthesize the metallic gray bulk of this compound very quickly (less than half hour!).

Caution! However, one must be careful because of a possible explosion of the reaction tube during heating caused by not only high vapor pressure of sulfur but also extremely exothermic reaction between the irons and the sulfurs. Therefore, until the sample is completely melted, you must put the reaction tube on the heat-resistant ceramics and heat it by direct flame with a protection shield.

(8) Haldane, F. D. M. *Phys. Rev. Lett.* **1983**, 50, 1153.
(9) Renard, J. P.; Verdaguer, M.; Regnault, L. P.; Erkelens, W. A. C.; Rossat-Mignod, J.; Stirling, W. G. *Europhys. Lett.* **1987**, *3*, 945.
(10) (a) Katsumata, K. *J. Magn. Magn. Mater.* **1995**, *140−144*, 1595 and references within. (b)Katsumata, K. *Curr. Opin. Solid State Mater. Sci.* **1997**, *2*, 226 and references within.
(11) Mutka, H.; Payen, C.; Molinié, P.; Escleston, R. S. *Physica B* **1995**, *213 & 214*, 170 and references within.
(12) (a)Todo, S.; Kato, K. *Phys. Rev. Lett.* **2001**, *87*, 047203-1. (b)Todo, S.; Matsumoto, M.; Yasuda, C.; Takayama, H. *Phys. Rev. B* **2001**, *64*, 224412.
(13) Granroth, G. E.; Meisel, M. W.; Chaparala, M.; Joliçur, Th.; Ward, B. H.; Talham, D. R. *Phys. Rev. Lett.* **1996**, *77*, 1616.
(14) Anthony, J. W., Bideaux, R. A., Bladh, K. W., Nichols, M. C., Eds.; *Handbook of Mineralogy*; Mineral Data Publishing: Tucson, AZ, 1990; Vol. 1.

Characterization. The phase relations of prepared samples were checked by powder X-ray diffraction (XRD) using Mac Science M21X (Cu Kα radiation, 45 kV, 350 mA). The morphological measurements and compositional analyses were verified by wavelength-dispersive spectrometer (WDS) analyses using a JEOL JSM-5600 scanning electron microscope (SEM) at a 15-kV accelerating voltage and a 1-min accumulation time per one position in which the corrections were made for atomic number, absorption, and fluorescence (ZAF). All of the samples for the physical measurements were carefully checked for homogeneity by these techniques before the measurements.

Differential Thermal Analysis. Differential thermal analysis (DTA) was performed with a Mac Science TG-DTA 2000 thermal analyzer. The ground samples were sealed in quartz ampules under vacuum (~10^{-5} Torr). As a reference, almost equal mass of α-Al_2O_3 in the quartz ampule with a vacuum seal was used. The samples were heated to 1100 °C at 10 °C/min and then isothermed for 5 min followed by cooling at 10 °C/min to room temperature. This process was repeated three times. After the DTA measurements, the samples were re-checked by XRD.

Crystallographic Studies. Before the intensity data collection for the crystal structure solution, the oscillation technique using Mo Kα X-ray at room temperature revealed that needle crystals grown by method A were aligned along the *c*-axis. A crystal with dimensions 0.020 × 0.015 × 0.200 mm was selected for intensity data measurement. The chemical composition measured by WDS was estimated at $FePb_{3.9(3)}Sb_{6.3(2)}S_{14.5(2)}$ from an average value of 20 different positions on the crystal. Intensity data at 296 K were collected up to $2\theta = 70°$ using the $\omega-2\theta$ scan mode with 8°/min on a RIGAKU AFC6S four-circle diffractometer equipped with a pyrolitic graphite monochromator and Mo Kα radiation (50 kV, 40 mA). The stability of the crystal was monitored by measuring three standard reflections periodically (every 150 reflections) during the course of data collection. To reduce the statistics error, intensity data of each weak reflection were repeatedly measured up to 10 times with hard criterion as $\sigma I/I = 0.01$, and the Friedel-pair reflections were also measured. Lp and a semiempirical absorption correction based on 10 Ψ-scan data were applied to the data.

The structure was solved by direct methods[17] and refined by full-matrix least-squares techniques on F^2 of the teXsan package.[17] The Fe site in the primary structure solution was located at a Wyckoff position, 2b ($^1/_2$, 0, $^1/_2$) in space group $P2_1/a$ and all of the other sites were at the general position 4e (*x*, *y*, *z*). To correspond with the previous structure model,[15] all of atom sites were shifted to ($-^1/_2$, 0, $-^1/_2$) and re-refined as the final structure. No disorder evidence was observed in each site. All atoms were refined anisotropically to give a final $R_1 = 3.2\%$. The crystallographic data and structural analysis are listed in Table 1. Final atomic coordinates are given in Table 2.

Optical Spectroscopy. Diffuse spectra were recorded for the fine powdered samples at room temperature. Optical diffuse reflectance measurements in the wave range of UV/visible/near-IR were made with a customized machine based on a Shimadzu UV-3100PC double-beam, double-monochromator spectrophotometer. The instrument was equipped with an integrating sphere. As a standard of 100% reflectance, $BaSO_4$ powder was used. Reflectance data were converted to the absorption data by the Kubelka−Munk function,[18]

$$\frac{\alpha}{S} = \frac{(1-R)^2}{2R} \quad (1)$$

where *R* is the reflectance at a given wavelength, α is the absorption coefficient, and *S* is the scattering coefficient. The scattering coefficient was treated as a constant because it has been shown to be independent of wavelength for a particle sufficiently large (>5 μm). The average particle size used for measurements is significantly large (>20 μm).

Charge-Transport Measurements. dc electrical resistivity for the polycrystalline pellets was measured by the usual four-probe technique with 25-μm gold wires as current voltage electrodes and gold paste to attach. Measurements were carried out in the temperature range 77−300 K by using a Quantum Design PPMS with an ac transport controller. The polycrystalline samples were sieved to obtain an average particle diameter of 20 μm and pelletized under an Ar atmosphere to avoid oxidation during the following the annealing process. Before measurements, the pelletized samples attached with electrodes were sealed in quartz tubes under vacuum and then were sintered at 400 °C for 24 h to be dense and reduce the grain boundary.

Magnetic Measurements. Magnetic susceptibility measurements were performed in the temperature range 1.8−385 K and at the

Table 1. Crystallographic Data and Structural Analysis for $FePb_4Sb_6S_{14}$

formula weight	2064.19
cryst. shape/color	needle/metallic gray
temp	296 K
space group	$P2_1/a$ (No. 14)
a	15.750(6) Å
b	19.125(3)
c	4.030(4)
β	91.68(8)°
V	1213(1) Å^3
Z	2
μ(Mo Kα)	35.981 mm^{-1}
D_c	5.651 g/cm^3
F_{000}	1768.0
no. measured reflns	5084
no. unique reflns	2314
no. observed reflns ($F^2 > 2.0\sigma(F^2)$)	1284
R_{int}	7.7%
final R1/wR ($F^2 > 2.0\sigma(F^2)$)	3.16/8.92%
GOF	0.742

Table 2. Fractional Atomic Coordinates and Isotropic Temperature Factors (Å^2) with Estimated Standard Deviations in Parentheses for $FePb_4Sb_6S_{14}$

site	*x*	*y*	*z*	U_{eq}
Pb1	−0.07429(6)	0.26108(2)	0.0556(1)	0.0211(3)
Pb2	−0.31702(6)	0.35932(3)	0.0341(1)	0.0233(3)
Sb1	0.1312(1)	0.34110(4)	−0.3872(2)	0.0201(4)
Sb2	−0.10379(10)	0.45257(4)	−0.3874(2)	0.0153(4)
Sb3	−0.17991(9)	0.06342(4)	0.4116(2)	0.0167(4)
Fe	0.0000	0.0000	0.0000	0.017(1)
S1	−0.2157(4)	0.4968(2)	0.0268(8)	0.015(1)
S2	−0.0796(4)	0.1056(1)	−0.0108(7)	0.018(2)
S3	0.0959(4)	0.0436(1)	−0.4770(7)	0.014(1)
S4	0.0516(4)	0.2307(1)	−0.4319(7)	0.019(1)
S5	−0.1833(4)	0.3414(1)	−0.4505(7)	0.016(1)
S6	0.0024(4)	0.3981(1)	0.0467(8)	0.017(1)
S7	−0.2747(4)	0.2038(2)	0.0747(8)	0.019(1)

(15) Niizeki, N.; Burger, M. J. *Z. Kristallogr.* **1957**, *109*, 161.
(16) Chang, L. L. Y.; Knowles, C. R. *Can. Mineral.* **1977**, *15*, 374.
(17) (a) *SIR92*: Altomare, A.; Cascarano, G.; Giacovazzo, C.; Guagliardi, A.; Burla, M. C.; Polidori, G.; Camalli, M. *J. Appl. Crystallogr.* **1994**, *27*, 435. (b)*teXsan: Single Crystal Structure Analysis Software*, Version 1.11; Molecular Structure Corporation: The Woodlands, TX, 2000.
(18) (a)Wendlandt, W. W.; Hecht, H. G. *Reflectance Spectroscopy*; Interscience Pub.: New York, 1966. (b)Kortuem, G. *Reflectance Spectroscopy*; Springer-Verlag: New York, 1969.

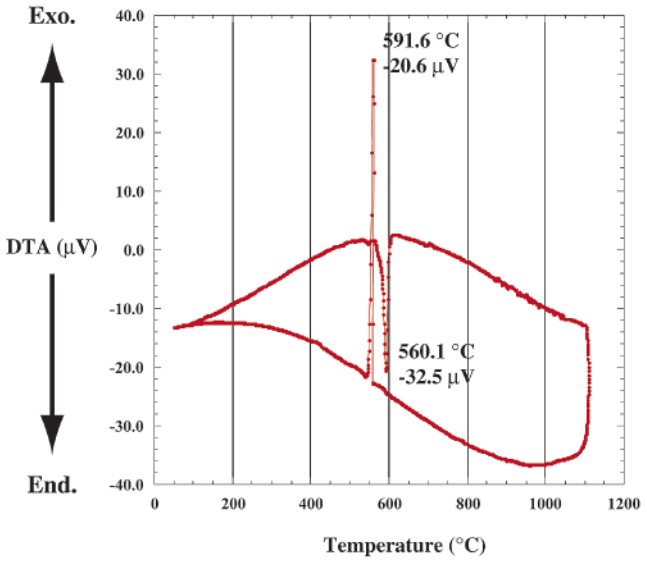

Figure 1. DTA curve for $FePb_4Sb_6S_{14}$ up to 1100 °C. Both the heating and cooling rates are 10 °C/min.

applied magnetic field of 0.01 T with zero-field cooling mode (ZFC) by using a Quantum Design 7T-MPMS-XL SQUID magnetometer. Unsieved polycrystalline samples were pelletized and placed in a gel cap sample holder.

III. Results and Discussion

Synthesis and Thermal Analysis. Under both synthesis methods (A and B), better synthesis of pure bulk $FePb_4Sb_6S_{14}$ was accomplished by reacting in the slightly iron-poor compositional range: Fe:Pb:Sb:S = 1:4.05−4.20:6.08−6.30:14.20−15.00 with long reaction time near 550 °C. Excess Pb−Sb−S materials (mainly $Pb_4Sb_6S_{13}$ and Sb_2S_3) sublimed at the lower temperature part of the reaction tube and could be easily removed during synthesis. In general, the reactivity between Fe−S at lower temperatures (<350 °C) is lower than that between Pb/Sb−S, and also the reaction speed between the iron sulfides and Pb/Sb sulfides is very slow. Non- or less-reacting materials with iron or iron sulfides have a tendency to form $Pb_4Sb_6S_{13}$ and/or Sb_2S_3 easily above 450 °C; these compounds melt with high volatility above ∼520 °C, and consequently ferromagnetic Fe_9S_8 is partially formed. For this reason, higher temperature syntheses (>520 °C) are needed to selectively form the slightly Pb−Sb−S-rich starting composition. The best starting composition to synthesize pure jamesonite bulk using method B is Fe:Pb:Sb:S = 1:4.15:6.28:14.90.

The thermal behavior of the jamesonite phase was investigated by differential thermal analysis (DTA). Jamesonite melts congruently at 592 °C and recrystallizes at 560 °C with a supercooling range of about 30 °C. In multiple heating and cooling cycles, jamesonite was confirmed to be a thermally stable phase (Figure 1).

In the present study, we could obtain only monoclinic jamesonite phase. No trace of orthorhombic parajamesonite phase was observed. The information on parajamesonite is too poor to identify it. Until now, there is a sole report with mineralogical information about parajamesonite because parajamesonite was produced from only one known locality,

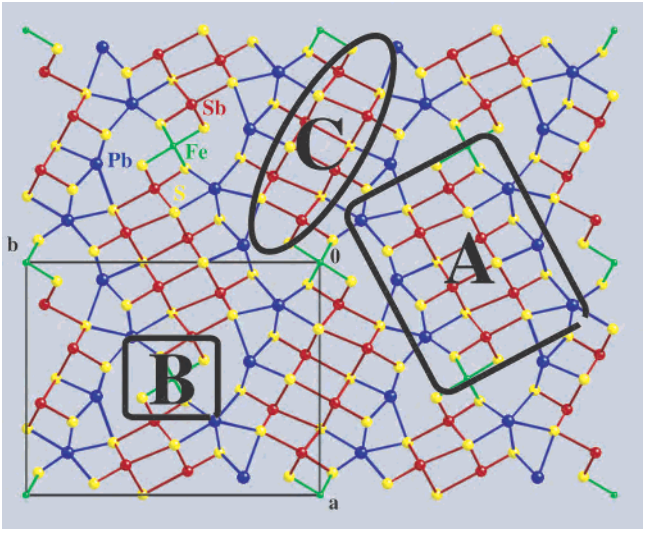

Figure 2. Crystal structure of $FePb_4Sb_6S_{14}$, jamesonite. View down the crystallographic *c*-axis of the unit cell showing two chains substructures {(A) $^3_\infty[Pb_4Sb_6S_{13}]$ and (B) $^1_\infty[FeS_6]$)} and (C) lone-electron pair micelle in A substructure. Red circle is Sb, blue is Pb, green is Fe, and yellow is S, respectively.

Herja, Rumania, as a rare mineral.[19] Recently, Cook and Damian reported that they could also not obtain any evidence of parajamesonite in the natural samples that came from the same locality.[20] Therefore, if the formula of parajamesonite is correct as $FePb_4Sb_6S_{14}$, parajamesonite is probably a metastable phase or a high-pressure form.

Description of Crystal Structure. The refined structure is shown in Figure 2. The basic crystal structure is the same as the previously reported model, but we obtained more accurate crystallographic details.[15] The structure consists of two components of rod-shaped substructures.

One is a Bi_2Te_3-type (or called SnS archetype); $^3_\infty[Pb_4Sb_6S_{13}]$ substructure (denoted as A in Figure 2) with a formal charge of +10 formed by all lead and antimony sites. In this substructure, lead atoms have slightly distorted triangular prism coordination. Lone-pair electrons (E) of Pb^{2+} are elongated to the pocket side where the other rod substructure, $^1_\infty[FeS_6]$, is formed. The coordination number (CN) is 7 for Pb1 and 8 for Pb2, and the mean bond distance is 3.016 Å for Pb1 with mono-capped trigonal prism coordination and 3.111 Å for Pb2 with bi-capped trigonal prism (Table 3 and Figure 3a,b). On the other hand, formal valence consideration suggests that all antimony atoms are trivalent. All antimony sites have a remarkably distorted coordination caused by active $5s^2$ lone-pair electrons (E) of Sb^{3+}. When we consider only shorter Sb−S bonds of about 3 Å, Sb1 and Sb3 have pseudo-tetrahedral pyramidal coordinations, SbS_4, and Sb2 has a pseudo-trihedral pyramidal one, SbS_3. If we consider that long Sb−S bonds, which are influenced strongly by the stereochemically active $5s^2$ lone-pair electrons (E) of Sb^{3+}, each coordination type for Sb is considered as distorted octahedral. However, in the Sb1 case, the sixth and seventh shortest bonds are to Sb3

(19) Zsivny, V.; Náray-Szabó, I. V. *Schweiz. Mineral. Petrogr. Mitt.* **1947**, *27*, 183.
(20) Cook, N. J.; Damian, G. S. *Geol. Carpathica* **1997**, *48*, 387.

Table 3. Selected Bond Distances (Å) under 4.0 Å with Estimated Standard Deviations in Parentheses for $FePb_4Sb_6S_{14}$

Pb1−	S4	2.880(4)	Sb2−	S5	2.476(3)
	S6	2.886(3)		S6	2.602(4)
	S4	2.891(4)		S1	2.603(4)
	S2	2.987(2)		S1	3.024(4)
	S5	3.043(3)		S6	3.051(4)
	S5	3.078(3)		S1	3.531(3)
	S7	3.344(5)		Sb2	3.870(2)
	ave.[a]	3.016 (CN = 7)		ave.[a]	2.560 (CN = 3)
				ave.[a]	2.881 (CN = 6)
Pb2−	S5	2.934(4) ×2	Sb3−	S3	2.447(3)
	S7	3.051(3)		S2	2.490(4)
	S3	3.061(3)		S1	2.698(4)
	S3	3.066(3)		S2	2.890(3)
	S1	3.076(4)		S1	3.110(4)
	S4	3.247(4)		S7	3.342(3)
	S4	3.484(4)		Fe	3.539(2)
	Fe	3.942(1)		Sb1	3.604(2)
	ave.[a]	3.111 (CN = 8)		Fe	3.838(1)
				ave.[a]	2.631 (CN = 4)
				ave.[a]	2.829 (CN = 6)
Sb1−	S4	2.459(4)	Fe−	S2	2.377(3) ×2
	S7	2.498(4)		S3	2.616(3) ×2
	S7	2.797(4)		S3	2.690(3) ×2
	S6	2.927(4)		Sb3	3.539(2) ×2
	S6	3.200(4)		Sb3	3.838(1) ×2
	Sb3	3.604(2)		Pb2	3.942(1) ×2
	S1	3.658(3)		ave.[a]	2.505 (CN = 6)
	ave.[a]	2.670 (CN = 4)			
	ave.[a]	2.776 (CN = 5)			

[a] "ave." means average bond distances calculated using the cation−anion bonds shorter than the cation−cation bonds. Coordination numbers (CN) are indicated in parentheses.

(3.604 Å) and S1 (3.658 Å), respectively. The local part in the $[Pb_4Sb_6S_{13}]$ substructure considered with these longer Sb−S bonds forms a so-called "*lone-electron pair micelle*",[21] which is denoted as C in Figure 2. The mean Sb−S bond distance, which is shorter than the sum of the van der Waals' radii[22] of Sb and S (3.80 Å), and CN are 2.776 Å and 5 for Sb1, 2.881 Å and 6 for Sb2, and 2.829 Å and 6 for Sb3 (Table 3 and Figure 3c−e). These distorted coordinations of Pb and Sb sites are commonly found in the crystal structures of sulfosalts containing these cations.[23]

These Pb and Sb polyhedra form the lozenge-shaped rod $[Pb_4Sb_6S_{13}]$ substructure that elongates parallel to the *c*-axis. The number of cations for the thickness (*N*) and width (*N*′) that periodically arranged in the $[Pb_4Sb_6S_{13}]$ substructure are 3 and 4, respectively. The characteristic $^3_\infty[Pb_4Sb_6S_{13}]$ framework is formed from each of this substructure connected by a kind of cell-twinning mechanism owing to the *a*-grid symmetrical operation of its space group, $P2_1/a$. Makovicky gives more details of classification for the crystal structures of complex sulfosalts.[24]

The other is a rod-shaped substructure (denoted as B in Figure 2), which forms by the FeS_6 octahedron. The octahedra form the 1D-infinite chain ($^1_\infty[FeS_6]$) with a formal charge of −10, which run parallel to the *c*-axis by sharing the edges of each octahedron (Figure 4a). This octahedron is slightly distorted from regular coordination: two shorter Fe−S bonds with S2 (2.377(4) Å) and four longer ones with S3 (2.616(4) Å × 2 and 2.690(4) Å × 2). This distortion (Figure 4b, Table 3) seems not to be caused by the Jahn−Teller effect with the electronic structure of Fe^{2+} ($t_{2g}^4e_g^2$) because a similar octahedral distortion has been observed in the isostructural Mn-end member bénavidésite, $MnPb_4Sb_6S_{14}$, with Mn^{2+} ($t_{2g}^3e_g^2$, $S = {}^5/_2$).[23j] It comes from strong covalency of Sb−S and Pb−S bonds. Antimony and lead atoms form a rigid framework $^3_\infty[Pb_4Sb_6S_{13}]$ with S atoms and Fe atoms fit into the octahedral voids in the framework. Therefore, the rigid $^3_\infty[Pb_4Sb_6S_{13}]$ framework governs the octahedral coordination surrounding Fe^{2+}. Similar octahedral coordinating distortions of transition metals in the sulfosalts having the single 1D transition metal chain are found in Mn-end member bénavidésite, $MnPb_4Sb_6S_{14}$ ($P2_1/a$),[23j] bérthierite, $FeSb_2S_4$ (*Pnma*),[25] clarite, $MnSb_2S_4$ (*Pnam*),[26] $Tl_2MnAs_2S_5$ (*Cmca*),[27] $CdBi_2S_4$ (*C*2/*m*),[28] $CdBi_4S_7$ (*C*2/*m*),[28] $Cd_{2.8}Bi_{8.1}S_{15}$ (*C*2/*m*),[28] $Cd_2Bi_6S_{11}$ (*C*2/*m*),[28] and $Mn_2Bi_{2.2}S_4$ (*C*2/*m*).[29] Mean Fe−S bond distance and coordination volume are 2.505 Å and 2.200 Å^3, respectively (Table 3).

The shortest Fe...Fe distance is 4.030(4) Å in the intrachain. Each $^1_\infty[FeS_6]$ chain is quite isolated by the $^3_\infty[Pb_4Sb_6S_{13}]$ framework substructure, which occupies the large area in the jamesonite crystal structure. Each Fe site between the $^1_\infty[FeS_6]$ chains is located in a topologically isophase. The first and second neighbor Fe...Fe distances in the interchain are 12.388(6) and 15.750(6) Å, respectively (Figure 4a). Therefore, the 1D magnetic property can be expected for this compound.

Optical Spectroscopy and Electrical Conductivity Measurements. Jamesonite absorbed all light in the UV/visible region. From the absorption edge in the near-IR region, the band gap, E_g, of jamesonite is estimated at 0.48 eV (Figure 5).

Electrical conductivity (σ) showed that jamesonite is an intrinsic semiconductor with 13 S/cm at 297 K. Below 100 K, its electrical conductivity reached the over-range of our instrument. Figure 6 shows a log σ vs $1/T$ plot. The activation energy, E_a, was estimated at 0.56 eV from the slope of this plot. This value is slightly larger than the estimated E_g from

(21) Makovicky, E.; Mumme M. *Neues Jahrb. Mineral., Abh.* **1983**, *147*, 58.

(22) Bondi, A. *J. Phys. Chem.* **1964**, *68*, 441.

(23) (a)See for example: Skowron, A.; Brown, I. D. *Acta Crystallogr.* **1990**, *C46*, 527. (b)Skowron, A.; Brown, I. D. *Acta Crystallogr.* **1990**, *C46*, 531.23. (c) Skowron, A.; Brown, I. D. *Acta Crystallogr.* **1990**, *C46*, 534. (d) Skowron, A.; Brown, I. D. *Acta Crystallogr.* **1990**, *C46*, 2287. (e) Skowron, A.; Brown, I. D.; Tilley, R. J. D. *J. Solid State Chem.* **1992**, *97*, 199. (f) Matsushita, Y.; Takéuchi, Y. *Z. Kristallogr.* **1994**, *209*, 475. (g)Skowron, A.; Boswell, F. W.; Corbett, J. M.; Taylor, N. J. *J. Solid State Chem.* **1994**, *112*, 251. (h) Skowron, A.; Boswell, F. W.; Corbett, J. M.; Taylor, N. J. *J. Solid State Chem.* **1994**, *112*, 307. (i)Matsushita, Y.; Nishi, F.; Takéuchi, Y. In *Tropochemical cell-twinning*; Takéuchi, Y., Ed.; Terra Publishing: Tokyo, Japan, 1997. (j)Matsushita, Y.; Ueda, Y. *Inorg. Chem.*, to be submitted.

(24) (a)Makovicky, E. *EMU Notes Mineral.* **1997**, *1*, 237. (b)Makovicky, E. *Eur. J. Mineral.* **1993**, *5*, 545.

(25) Lukaszewicz, K.; Pietraszko, A.; Stepien-Damm, J.; Kajokas, A.; Grigas, J.; Drulis, H. *J. Solid State Chem.* **2001**, *162*, 79.

(26) Bente, K.; Edenharter, A. Z. *Kristallogr.* **1989**, *186*, 31.

(27) Gostojic, M.; Edenharter, A.; Nowacki, W.; Engel, P. *Z. Kristallogr.* **1982**, *158*, 43.

(28) Choe, W. Y.; Lee, S.; Oconnell, P.; Covey, A. *Chem. Mater.* **1997**, *9*, 2025.

(29) Lee, S.; Fischer, E.; Czerniak, J.; Nagasundaram, N. *J. Alloys Compd.* **1993**, *197*, 1.

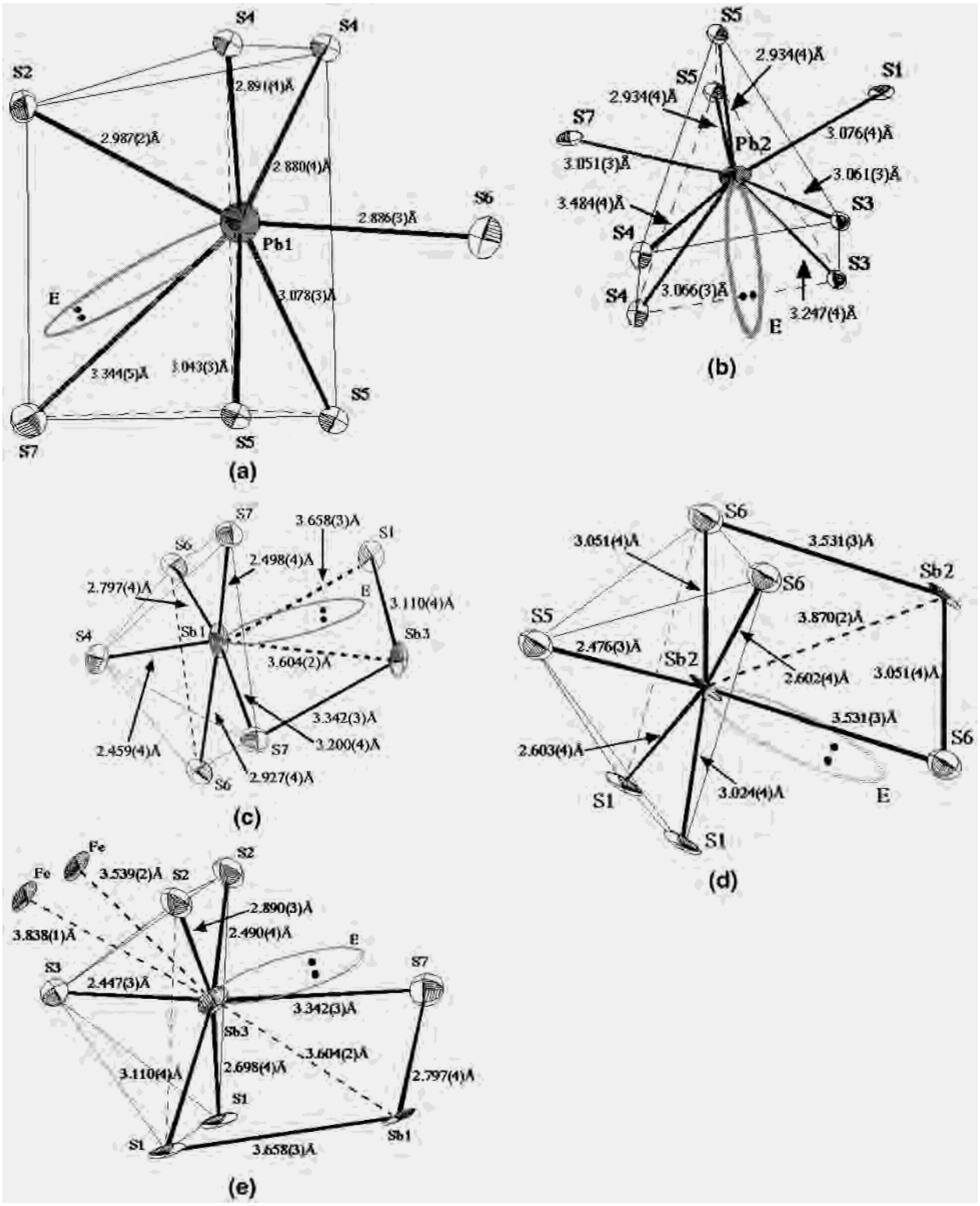

Figure 3. ORTEP drawing of stereochemical coordination types of Pb^{2+} and Sb^{3+} in $FePb_4Sb_6S_{14}$, jamesonite crystal structure. Bold dotted bonds are indicated short cation−cation distances and also presented cation−anion distances over cation−cation distances. Thin lines show coordination polyhedra of a trigonal prism for Pb and square pyramid for Sb, respectively. Lone-pair electron cloud is also presented as E. (a) Pb1 site, (b) Pb2, (c) Sb1, (d) Sb2, and (e) Sb3, respectively.

the optical absorbance because electrical conductivity is influenced by the grain boundaries and/or the surface conditions of the sample.

Therefore, we consider that the band gap value of jamesonite obtained by optics is more essential. This value of the band gap, 0.48 eV, is in good agreement with that of PbS (0.41 eV).[30]

Magnetic Susceptibility Measurements. Temperature dependence of molar magnetic susceptibility (χ_M) is shown in Figure 7a. Starting from $\chi_M \sim 0.006$ emu/mol at an applied

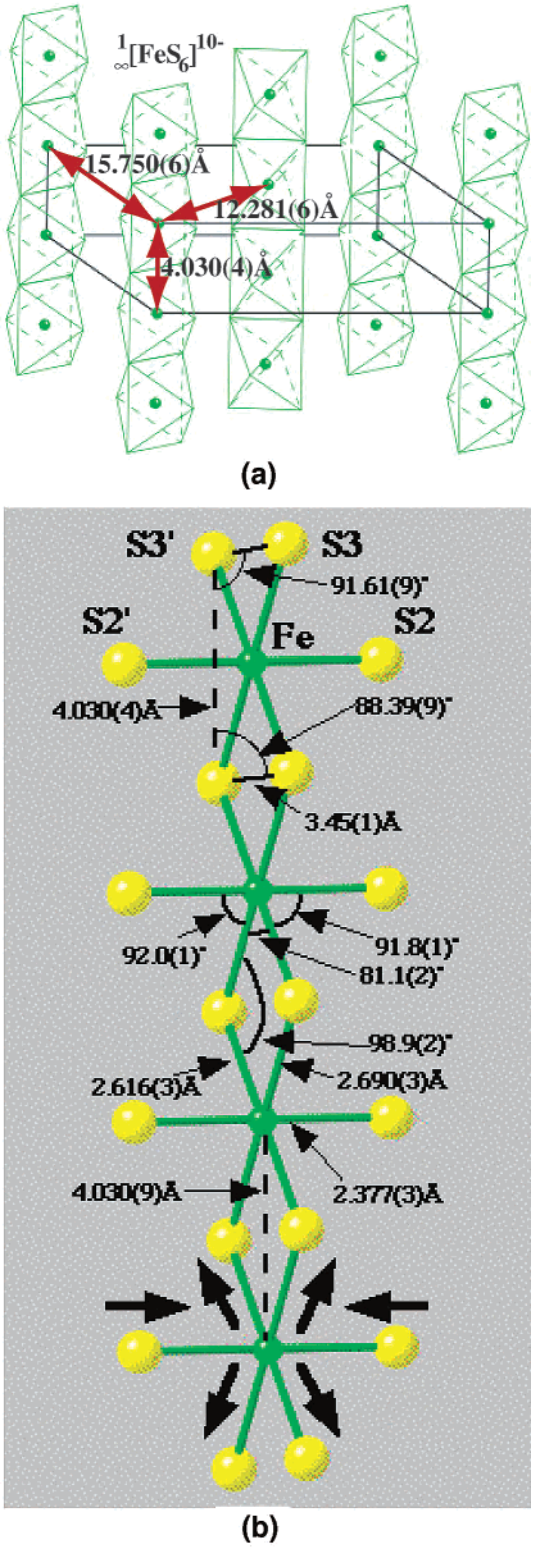

Figure 4. (a). Polyhedron drawing of the $^1_\infty[FeS_6]$ chain substructures in the unit cell and the short Fe···Fe interaction distances of inter- and intrachains. (b) Bond distances and angles in the $^1_\infty[FeS_6]$ chain substructure. Large arrows show distortion direction.

magnetic field of 0.01 T and 385 K, it increases with decreasing temperature, reaches a broad maximum of χ_M ~0.038 emu/mol at 33.5 K, and then decreases rather sharply below 33 K. The observed χ_M-T curve shows specific behavior for a low-dimensional magnet in which the broad peak is caused by the development of short-range magnetic ordering in the 1D-HAF chain. Above 120 K, the paramagnetic susceptibility obeys a Curie−Weiss law:

$$\chi_M = \frac{C}{(T-\theta)} + \chi_0 \qquad (2)$$

where $C = 2.43(2)$ is a Curie constant, $\theta = -8.0(7)$ K is Weiss temperature, and $\chi_0 = 0.0004(4)$ emu/mol is a constant term. The estimated effective magnetic moment (p_{eff}) from C is 4.41 μ_B, which bears out that Fe^{2+} in jamesonite exists in a high-spin state ($t_{2g}^4e_g^2$, $S = 2$), although it is slightly lower than the calculated p_{eff} (4.90 μ_B) for high-spin Fe^{2+}.[31]

The Heisenberg Hamiltonian [eq 3] gives the magnetic behavior for a 1D chain of interacting isotropic spins. We tried to fit the observed χ_M to the approximate equation for

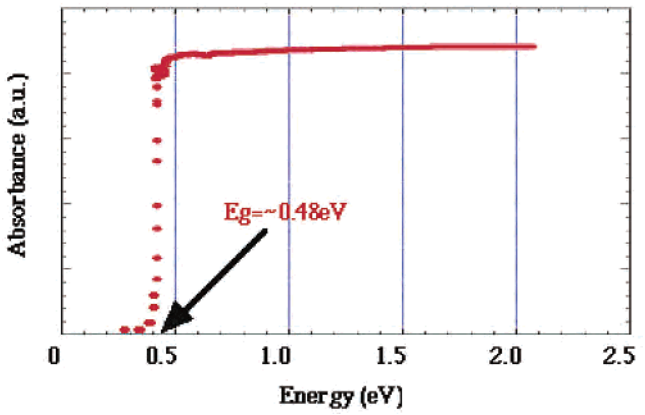

Figure 5. Optical absorption spectrum for powdered $FePb_4Sb_6S_{14}$, jamesonite, measured at room temperature.

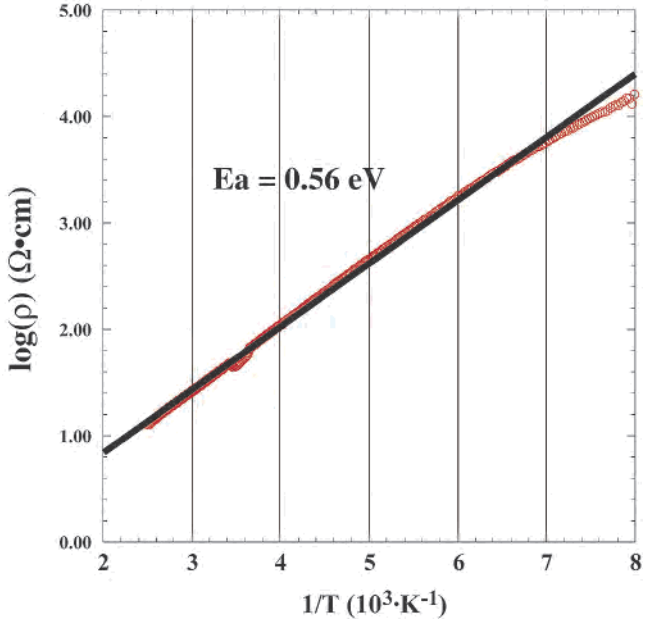

Figure 6. Arrhenius plot of electrical conductivity for polycrystalline $FePb_4Sb_6S_{14}$, jamesonite. Black straight line shows least-squares linear fit to estimate the activation energy (E_a).

(30) Berger, L. I. *Semiconductor Materials*; CRC Press: Boca Raton, FL, 1997.
(31) West, A. R. *Solid State Chemistry and Its Applications*; John Wiley & Sons: Chichester, 1984.

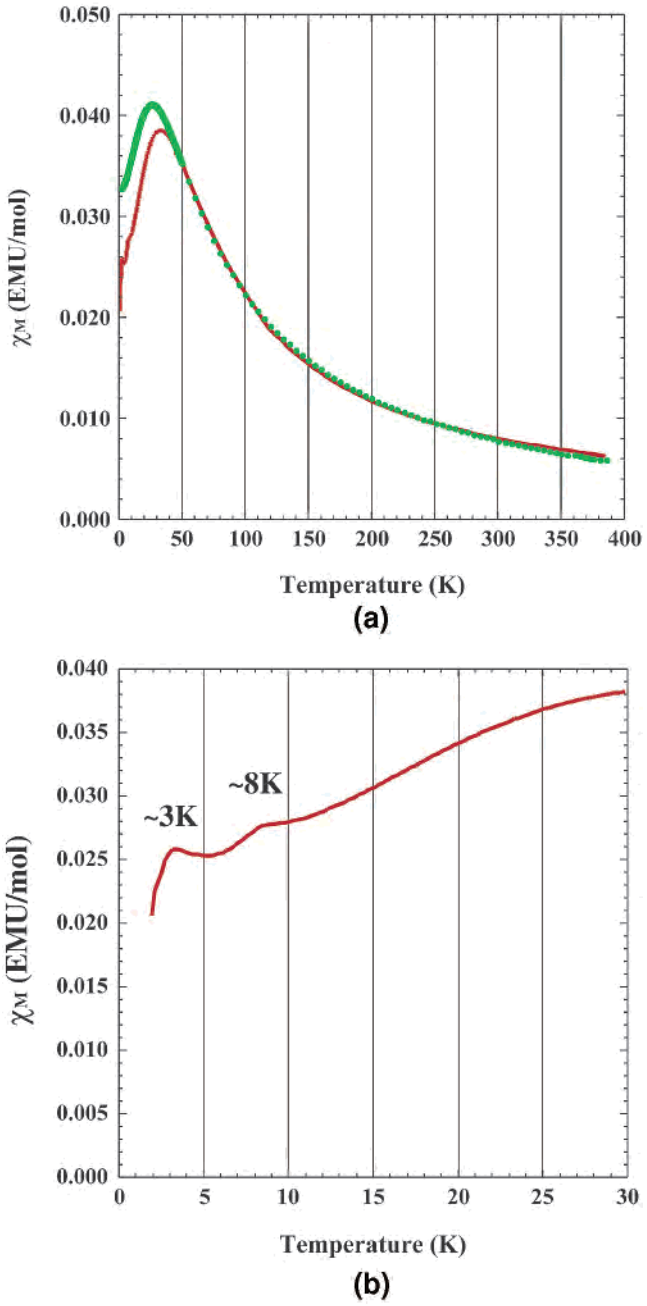

Figure 7. (a) Molar magnetic susceptibilities measured in a magnetic field of 0.01 T. Green dotted line indicates a fit using Hiller's 1D-HAF function. (b) Molar magnetic susceptibilities measured in a magnetic field of 0.01 T, below 10 K. Two anomalies are shown around 8 and 3 K, respectively.

the behavior of a quantum spin HAF chain, which was published by Hiller et al. [eqs 4 and 5].[32]

$$H = -2J\sum_{i\neq j} S_i \cdot S_j \tag{3}$$

$$\chi_M = \left[\frac{(Ng^2\mu_B{}^2)}{k_B T}\right]\cdot\left[\frac{(A + Bx^2)}{(1 + Cx + Dx^3)}\right] \tag{4}$$

$$x = \frac{|J|}{k_B T} \tag{5}$$

where N is Avogadro's number, g is Landé's factor, μ_B is Bohr magneton, and k_B is Boltzmann's constant, respectively. Each coefficient for $S = 2$ given by Hiller et al. is $A = 2.0000$, $B = 71.938$, $C = 10.482$, and $D = 955.56$, respectively.[32] After adding a constant term (χ_0) to this equation, we tried to fit the raw data to the equation. A reasonable least-squares fit was not obtained in the whole temperature range measured. In general, the real χ_M behavior does not show an ideal one, especially in the low-temperature region, because an ideal isolated chain is rare in the real system and there exists finite interactions between chains or to the second and third neighbors in intra- and interchains. The solid line in Figure 7a shows the best fit in the higher temperature region. As shown in Figure 7a, this numerical approach reproduces the observed χ_M behavior, especially the χ_M is well-fitted to the theoretical curve above 60 K, and it deviates from that below 60 K. This suggests that the titled compound is a good 1D-HAF magnet with $S = 2$. The deviation of χ_M from the ideal one suggests an existence of finite interchain interaction. From this fitting, we obtain a value of $g = 2.100(10)$, $|J|/k_B = 3.60(4)$ cm^{-1} (=5.18 K), and $\chi_0 = -0.0020(1)$ emu/mol, respectively. We also examined fitting the magnetic susceptibility data with the Ising model on trial, but we could not obtain any reasonable values.

Below the maximum point around 33.5 K, χ_M decreases somewhat sharply, compared with the theoretical curve. Figure 7b shows the temperature dependence of χ_M below 30 K. Two anomalies at ~8 and ~3 K, respectively, are observed and the χ_M decreases rapidly toward zero at 0 K below the second anomaly at ~3 K, suggesting any magnetic ordering or a spin-gapped ground state, that is, an $S = 2$ Haldane system. In preliminary heat capacity measurements, we could not observe any peaks in the whole temperature range down to 0.4 K. Therefore, we conclude that these anomalies observed in a lower temperature range are not due to the magnetic ordering. The theoretical calculation for the $S = 2$ Haldane system predicts the energy gap $\Delta_{S=2} = 0.09$ J. We obtained $|J|/k_B = 5.18$ K from fitting the χ_M to eq 4. By using this J value, we can estimate $\Delta_{S=2} = 0.47$ K, far below the lowest temperature (2 K) in the present χ_M measurement. Therefore, a gapped state as the ground state has been an open question.

To understand the magnetic energy state for this compound, we are trying to measure the magnetic susceptibilities down to the much lower temperature range (<0.4 K), the magnetization up to a high-magnetic field (<60 T), and also the magnetic spin relaxations under a lower temperature range (<0.4 K) by μSR measurements.

IV. Concluding Remarks

In summary, we successfully synthesized pure $FePb_4Sb_6S_{14}$, monoclinic jamesonite phase, and investigated its crystal structure and thermal, optical, and electromagnetic properties. It congruently melts at 592 °C. By an isothermed

(32) Hiller, W.; Strähle, J.; Datz, A.; Hanack, M.; Hatfield, W. E.; ter Haar, L. E.; Gütlich, P. *J. Am. Chem. Soc.* **1984**, *106*, 329.

and slowly cooling process near the melting point, we obtained needlelike crystals on the bulk surface. Moreover, we developed a new synthetic method for this compound to reduce the reaction time dramatically. In our study, we could not observe any evidence of the existence of an orthorhombic parajamesonite phase. Results of refinement of the crystal structure show that this compound has two substructures: $^{3}_{\infty}[Pb_4Sb_6S_{13}]$ and $^{1}_{\infty}[FeS_6]$. Both substructures are running parallel to the *c*-axis. The former structure is the lozenge-shaped Bi_2Te_3-type (or SnS archetype) and is formed from the $^{3}_{\infty}[Pb_4Sb_6S_{13}]$ substructures connected by a kind of cell-twinning mechanism with the *a*-grid of $P2_1/a$. The latter one is a novel single 1D-magnetic straight linear chain formed by the edge-shared $Fe^{2+}S_6$ octahedra. The octahedron is distorted by strong covalency of Sb−S and Pb−S bonds where S atoms are shared between Fe and Sb or Pb. Each $^{1}_{\infty}[FeS_6]$ chain is quite isolated by the $^{3}_{\infty}[Pb_4Sb_6S_{13}]$ framework, and the phase of this chain is topologically the same. From low electrical conductivities, this compound is an intrinsic semiconductor with an optical band gap, ∼0.48 eV. In the magnetic measurements, we found 1D-HAF behavior, as expected from the specific crystallographic features. Above 120 K, the magnetic susceptibility obeys a Curie−Weiss law, and the estimated effective moment (p_{eff}) from the Curie constant bears out that Fe^{2+} exists in a high-spin state ($t_{2g}^4e_g^2$, $S = 2$). Below 120 K, it shows a broad peak caused by the development of magnetically short-range order at 33.5 K and two additional anomalies at ∼8 and ∼3 K. The temperature dependence of magnetic susceptibility obeys well a theoretical curve for an $S = 2$ 1D-HAF system, except for the deviation below 60 K. The rapid decrease of magnetic susceptibility below 3 K suggests a gapped state as the ground state, which is a possible $S = 2$ Haldane system.

Acknowledgment. The authors thank Prof. Z. Hiroi, Drs. M. Isobe, H. Kageyama, and K. Nozawa (ISSP) for the various fruitful helps for the magnetic measurements, and to Dr. Z. Zhou (AIST, Tsukuba) for the optical measurements. This work is partly supported by Grants-in-Aid for Scientific Research (No. 407 and No. 758) and for Creative Scientific Research (No. 13NP0201) from the Ministry of Education, Culture, Sports, Science, and Technology. We also most gratefully acknowledge Komatsu Ltd. Co. for financial support.

Note Added in Proof

After the present work was submitted for publication, an independent study of this compound, $FePb_4Sb_6S_{14}$, jamesonite was published by P. Léone et al. (*Solid State Sci.* **2003**, *5* (5), 771−776), reporting brief results of re-determination of the crystal structure and brief magnetic susceptibility using natural mineral sample without detail of interactions.

Supporting Information Available: Crystallographic information for this compound is available as a CIF file. This material is available free of charge via the Internet at http://pubs.acs.org.

IC034634T